A Toughness Study of Steel Weld Metal From Self-Shielded Flux-Cored Electrodes—Part I

Weld metal toughness comparable to that obtained with shielded metal-arc electrodes is possible when a minimum of killing agents is retained in solid solution in the weld deposit

BY D. J. KOTECKI AND R. A. MOLL

ABSTRACT. The principal difficulty with commercially available self-shielded flux-cored electrodes is the lack of notch toughness in the resulting weld deposit. The objective of this investigation was to determine the factors contributing to this problem. In particular, a systematic study was made of the effects of microstructure, unconsumed killing agents which enter solid solution, and the presence or absence of air in the arc environment. Both commercially available electrodes and synthetic electrodes were used in this study.

The results show that the most important factor contributing to poor notch toughness is the dual effect of unconsumed killing agents (silicon, aluminum, and/or titanium). First, killing agents in solid solution have a hardening effect which raises Charpy vee-notch transition temperature. Second, the killing agents, especially aluminum and titanium, have the ability to alter the sequence of metallurgical transformations.

With small amounts of killing agents, transformation of austenite to tough fine ferrite is possible. In larger amounts, the killing agents favor the formation of relatively brittle bainite. In still larger amounts, the killing agents prevent austenite formation entirely, resulting in a coarse, brittle delta-ferrite structure formed during solidification and retained to room temperature. In comparison to these two effects, the effect of air in the arc environment is small.

Background

The evolution of electrodes for the deposition of steel weld metal has continued for more than half a century. Much of this evolution has been concerned with minimizing the detrimental effects of oxygen and nitrogen from the atmosphere and from the metal itself. The early bare electrodes left porous deposits due to the formation of gas bubbles during solidification of the weld pool. Covered electrodes were eventually developed which produced gases, and later slag, which displaced the atmospheric oxygen and nitrogen. More recently, elements such as silicon and manganese have been added to shielded metal-arc electrodes to combine with any remaining oxygen or nitrogen in nonharmful forms. This evolution of shielded metal-arc electrodes has progressed to the point that strength, ductility, and notch toughness equal to or greater than that of commercial high quality mild or low-alloy steels can be obtained with electrodes such as AWS-ASTM E7018.[1]

Recently, electrode development has concentrated in the area of continuous electrodes for the gas metal-arc and flux-cored metal-arc processes because of their higher deposition rates as compared with the shielded metal-arc process. These processes require electrical contact along the entire length of the electrode, so that coating of the electrode is not feasible. Initially, an externally-supplied shielding gas was introduced to exclude the atmosphere from the arc area and cover the weld pool as it solidified. The addition of deoxidizers (primarily manganese) to the wire was also required. More recently, tubular electrodes for gas shielded flux-cored metal-arc welding were developed; these allowed the deoxidizers and some slag-forming materials to be placed inside the electrode.

The gas shielded flux-cored metal-arc process produces a strong, ductile, tough steel deposit.[2] In addition, less welder skill is required for quality weldments, and much higher deposition rates are possible than with the shielded metal-arc process. But the need for externally supplied shielding gas complicates the process and makes it less portable than shielded metal-arc welding. Furthermore, the method is sensitive to drafts which may blow away the shielding gas.[3–5]

Some attempts were made to produce a flux-cored electrode which was a true "inside-out" shielded metal-arc electrode (containing gas-formers as well as slag-formers and deoxidizers) not requiring externally-supplied shielding gas, but these met with failure. The failure was due to the decomposition of shielded metal-arc electrode coating materials like calcium carbonate, which starts at approximately 1000° F, much below the melting temperature of the enclosing wire. The result is gas pressure within the wire which causes excessive spattering of molten metal.[5]

In 1959 a patent[4] was granted for what has come to be known as "self-shielded flux-cored electrodes." With this type of electrode a partial displacement of atmospheric oxygen and nitrogen is obtained by vaporization of halide salts such as lithium fluoride or calcium fluoride in the arc along with a slag covering the weld pool as it solidifies. Oxygen and nitrogen which enter the weld pool are consumed by deoxidizers (primarily manganese) and killing agents such as silicon, aluminum, titanium, boron, and/or zirconium. (The distinction between "deoxidizers" and "killing agents" is that the former are materi-

D. J. KOTECKI is a Ph. D. candidate, Dept. of Mechanical Engineering, and R. A. Moll is Assistant Professor, Dept. of Mechanical Engineering and Metallurgical Engineering, The University of Wisconsin, Madison, Wis.

Paper to be presented at the AWS 51st Annual Meeting in Cleveland, Ohio, during April 20-24, 1970.

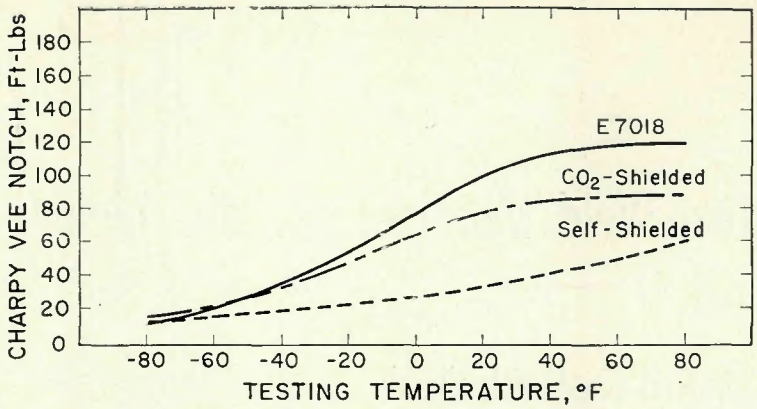

Fig. 1—Charpy V-notch energy as a function of temperature for a shielded metal-arc deposit,[1] a gas-shielded flux-cored electrode deposit,[2] and a self-shielded flux-cored electrode deposit[2]

als having greater affinity for oxygen than iron has, but less affinity for oxygen than carbon has; the latter are materials having a greater affinity for oxygen than either iron or carbon. Killing agents also form nitrides.[4])

With these electrodes, weld metal strength and ductility are adequate for many steel applications, but weld metal notch toughness is poor as compared to that of high quality shielded metal-arc or gas metal-arc steel deposits—Fig. 1. In addition, nothing of a quantitative nature regarding the mechanisms responsible for the poor notch toughness has appeared in the literature.

More recently, self-shielded flux-cored electrodes using small nickel additions have been developed. Although these electrodes have improved toughness characteristics, they also have higher hardenability and the nickel content exceeds AWS specifications for E70T5 deposits.

Objectives

Self-shielded flux-cored electrodes have been commercially available for about 10 years, and their lack of toughness is generally recognized to be a problem.[2, 5] But the reasons for this toughness problem are not well documented in the literature.

It has been suggested[5] that one of the reasons for the high transition temperature range from brittle to ductile fracture is the presence of oxide and nitride particles in the weld deposit, formed by the reaction of deoxidizers and killing agents with the atmosphere. Presumably, these particles, being hard and brittle, act as crack initiators during local yielding of the ferrous matrix. Aluminum nitride is thought to be especially harmful.[5]

On the other hand, it has also been suggested[6] that the chemical nature of inclusions in steel weld metal is of secondary importance as regards toughness. According to this approach, the critical factor in determining toughness is the ratio of particle size to particle spacing, with a low ratio favoring good toughness.

Still another study[7] of particles in steel weld metal, albeit deposited by the shielded metal-arc process, showed nonmetallic particles in welds which exhibited poor toughness. Subsequent heat treatment improved toughness, and no evidence was found to indicate that the particles had any effect on mechanical properties. Instead, property changes were attributed to changes in the structure and substructure of the ferrous matrix and to the presence or absence of grain boundary carbides. Other researchers[8] have found that inclusions or precipitates affect the ductile fracture energy, but not the transition range, of some steels.

Another suggested cause of poor weld metal toughness in self-shielded flux-cored electrode deposits is the effect of excess killing agents beyond that needed to consume oxygen and nitrogen.[5] These can enter into solid solution in the ferrous matrix and thereby alter its mechanical properties. For example, silicon in excess of 0.3% is reported to increase transition temperatures in steel plates by 125° F per weight per cent.[9] On the other hand, an increase of only 14° F per weight per cent of silicon has been reported for shielded metal-arc electrode deposits.[10]

Table 3—Flux Analysis of Commercial Electrode, %

SiO_2	0.50
Al	15.83
CaF_2	67.00
MgO	11.70
K_2O	0.59
Na_2O	0.17
C (Total)	1.25
Mn	2.90
Fe	3.55

Table 1—Basis of Experimental Electrode Flux, %

Fluorspar (CaF_2)	25
Sodium titanate (20% Na_2O, 40% TiO_2, 22% MnO, 18% SiO_2)	2
Electrolytic Mn	4.5
Calcium carbonate ($CaCO_3$)	2
Iron powder	Balance

Table 2.—Killing Agent Additions to Experimental Electrode Flux, %

Electrode no.	FeSi (50% Si)	Al	FeTi (40% Ti)
S-1	5	0	0
S-2	9	0	0
SA-1	5	4	0
SA-2	9	4	0
ST-1	5	0	6
ST-2	9	0	6
SAT-1	5	4	6
SAT-2	9	4	6
SAT-3	7	2	3

In view of these disagreements it was decided to study—in a quantitative manner—the effects of air-killing agent reaction products, metallurgical structure, and solid solution of surplus killing agents on the transition temperature ranges of steel weld metal deposited from self-shielded flux-cored electrodes.

In order to study these effects in an efficient manner, particularly solid solution effects of surplus killing agents, it was decided to fabricate a number of experimental self-shielded flux-cored electrodes. It should be pointed out that these wires were not designed to directly develop an electrode with improved toughness over that commercially available. Developments of this sort are the concern of electrode manufacturers. Rather, it is felt that these results could prove useful to both electrode manufacturers, in their continuing development of improved self-shielded flux-cored electrodes, and to electrode users as well, in their own evaluations of self-shielded flux-cored deposits.

Experimental Method

Materials

Nine electrodes were fabricated of such core chemistry as to constitute a 2^3 factorial design plus the center point. The design variables were the silicon, aluminum, and titanium content of the electrode flux. Those three elements are the most widely used killing agents in commercial self-shielded flux-cored electrodes. The base analysis of the experimental electrode flux is given in Table 1.

The specific killing agent additions

Table 4—Electrode Tube and Base Metal Steel Analyses, %

	C	Mn	Si	P	S
Experimental electrodes	0.08	0.43	.01	.020	.012
Commercial electrode	0.082	0.43	—	.004	.011
Base metal	0.15	1.28	.05	.026	.028

to the flux are listed in Table 2. These additions were made by replacing iron powder with ferro-silicon, aluminum, and ferro-titanium to maintain the same base analysis of everything but iron.

The flux of the commercially available wire used in this study was also analyzed. These results are given in Table 3.

Both the experimental electrodes and the commercial electrode were $^3/_{32}$ in. in diameter. The flux comprised 28-30% of the total weight of the experimental electrodes and 18% of the commercial electrode. The analyses of the steel tube portion of both types of electrodes and of the base metal on which welds were deposited are given in Table 4.

Welding Procedure

Two pass weldments were produced in single-U joint preparations as sketched in Fig. 2. The first pass weld completely filled the original groove in the plate. A second, smaller groove as then milled into the first pass, and this groove was completely filled by the second pass. This technique provides a weld with minimum base metal dilution, no recrystallized regions, and a geometry suitable for machining all-weld-metal tensile specimens and half-thickness Charpy vee notch specimens.

A 500 amp, 100% duty cycle, constant potential power source and a side-beam electrode holder carriage were used for weld deposition. Welding conditions were obtained by considering recommended conditions for the commercial electrode and adjusting to somewhat lower voltage to compensate for the sensitivity of the silicon-killed experimental wires (S-1 and S-2) to voltage. The conditions arrived at are listed in Table 5. Higher voltage tended to produce macroporosity in the silicon-killed welds.

Two test weldments were made with each electrode, one in air and the other with a shielding gas. The shielded welds were made to aid in observing the effects of nitrides on weld metal toughness. Originally, it was intended to use argon as the shielding gas; however, the five experimental wires containing titanium would not "wet" the base metal in argon under the welding conditions listed in Table 5. Therefore, to overcome this difficulty, 7% oxygen had to be added to the shielding argon for those five electrodes.

Table 5—Standardized Welding Conditions for Experimental and Commercial Electrodes

Electrode feed speed, ipm	196
Open circuit voltage, v	$30^1/_2$
Average load voltage, v	26
Average arc current, amp	320 amperes
Electrical stick-out, in.[a]	$2^1/_2$
Electrode angle to plate surface[a]	30 deg dragging
First pass electrode holder speed, ipm	7
Second pass electrode holder speed, ipm	9

[a] See Fig. 3.

The shielding method and electrode holder orientation are sketched in Fig. 3. The gas cup was not present during self-shielded welding.

Specimen Preparation

Approximately 25 half-thickness Charpy vee notch specimens, two $^1/_8$ in. all-weld-metal tensile specimens, and metallographic specimens were machined from each test weld. Twenty-five gram samples from each weld were used for bulk analysis.

Solid solution of manganese, sili-

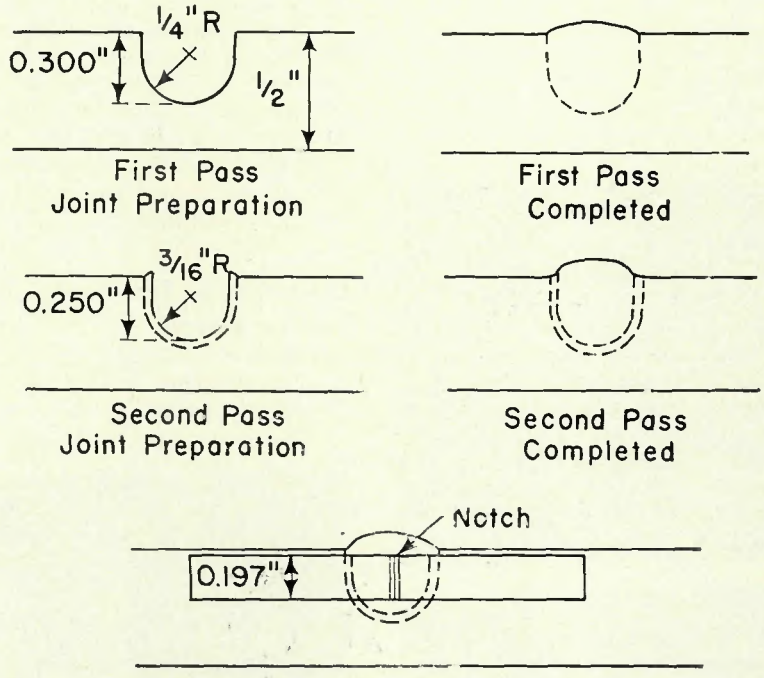

Fig. 2—Joint preparation used for test welds and location of half-width Charpy V-notch specimens

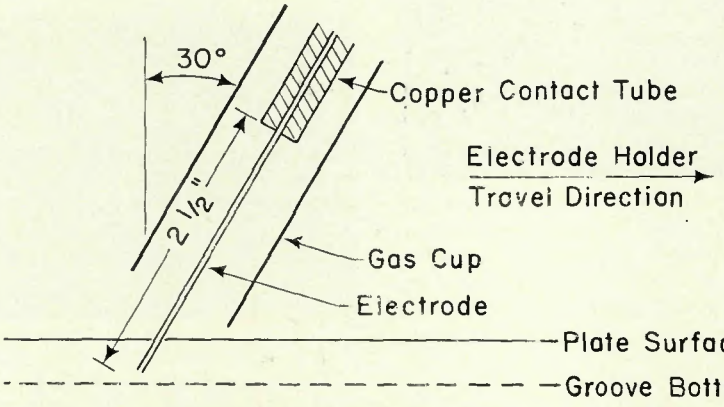

Fig. 3—Schematic of geometrical relationship between electrode holder and work piece during test welding

Table 6—Chemical Analysis of Weld Deposits, %

Electrode	Arc environment	Bulk analysis C	P	S	Mn	Si	Al	Ti	Matrix analysis (probe) Mn	Si	Al	Ti
S-1	Argon	.070	.010	.023	1.51	0.58	—	—	1.669	0.614	—	—
	Air	.083	.010	.022	1.40	0.50	—	—	1.554	0.558	—	—
S-2	Argon	.065	.010	.022	1.63	1.20	—	—	1.769	1.337	—	—
	Air	.060	.010	.023	1.51	1.17	—	—	1.739	1.202	—	—
SA-1	Argon	.106	.011	.014	1.76	0.84	0.60	—	1.890	0.903	0.704	—
	Air	.115	.010	.014	1.75	0.82	0.38	—	1.728	0.807	0.505	—
SA-2	Argon	.078	.007	.011	1.81	1.48	0.56	—	1.863	1.452	0.569	—
	Air	.083	.008	.011	1.80	1.40	0.37	—	1.813	1.380	0.358	—
ST-1	Argon+7% O_2	.051	.009	.014	1.83	0.81	—	0.22	1.724	0.837	—	0.129
	Air	.064	.008	.012	1.72	0.73	—	0.16	1.792	0.844	—	0.029
ST-2	Argon+7% O_2	.056	.008	.017	1.87	1.46	—	0.25	1.887	1.626	—	0.136
	Air	.064	.008	.014	1.80	1.48	—	0.24	1.894	1.608	—	0.100
SAT-1	Argon+7% O_2	.064	.007	.011	1.83	0.91	0.66	0.72	1.919	0.974	0.741	0.574
	Air	.069	.009	.010	1.85	0.91	0.58	0.67	1.887	0.988	0.737	0.426
SAT-2	Argon+7% O_2	.061	.009	.016	1.87	1.62	0.85	0.76	1.931	1.499	0.780	0.625
	Air	.064	.009	.012	1.84	1.53	0.68	0.67	1.873	1.416	0.707	0.421
SAT-3	Argon+7% O_2	.065	.008	.016	1.86	1.22	0.20	0.28	1.903	1.135	0.227	0.272
	Air	.055	.008	.014	1.79	1.14	0.16	0.25	1.982	1.159	0.250	0.155
Commercial	Argon	.243	.010	.005	0.98	0.15	2.20	—	0.991	0.183	2.010	—
	Air	.198	.009	.007	0.94	0.13	1.40	—	0.911	0.181	1.589	—

con, aluminum, and titanium in the ferrous matrix (independent of the quantities of these elements contained in inclusions in the weld metal) was measured with an electron beam microprobe analyzer. The X-ray count data for manganese and titanium were corrected for absorption and flouresecence effects using the combined methods of Philibert[11] and Reed.[12] The X-ray count data for aluminum and silicon were corrected for atomic number effects according to the method of Thomas.[13]

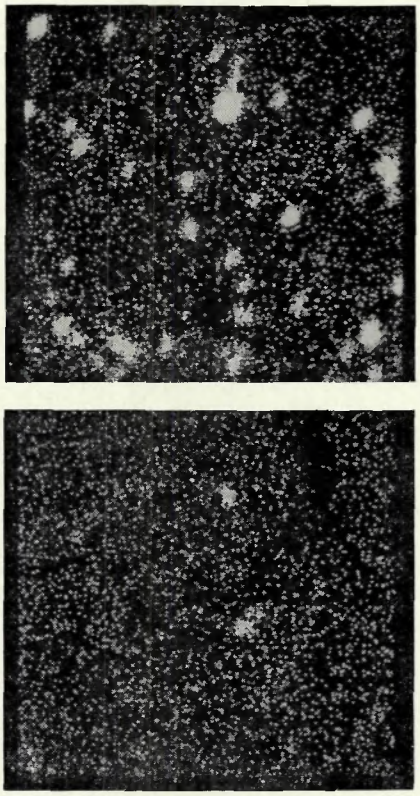

Fig. 4—Particle distributions on Charpy V-notch fracture surfaces. A (top)—titanium X-rays from ST-1 in air; B (bottom)—aluminum X-rays from SA-1 in air. Electron probe operating conditions: 15 kv, 0.10 micro-amp. The particle size is somewhat exaggerated because the relatively high beam current and low excitation potential produces a large diameter beam (greater than 1 micron). X1000 (reduced 28% on reproduction)

Experimental Results

Chemical Analysis

The chemical analysis of the weld deposits obtained by electron probe analysis and bulk chemical analysis are presented in Table 6. The differences in the results are primarily due to differences in sampling method. The bulk analysis samples constituted the entire cross-section of the weld while the probe samples were confined to the region of the notch for Charpy specimens. In addition, probe data are more sensitive to macrosegregation effects.

The differences obtained in titanium content by the two methods is of particular interest. In this case, the probe analysis is consistently less than the bulk analysis because the probe

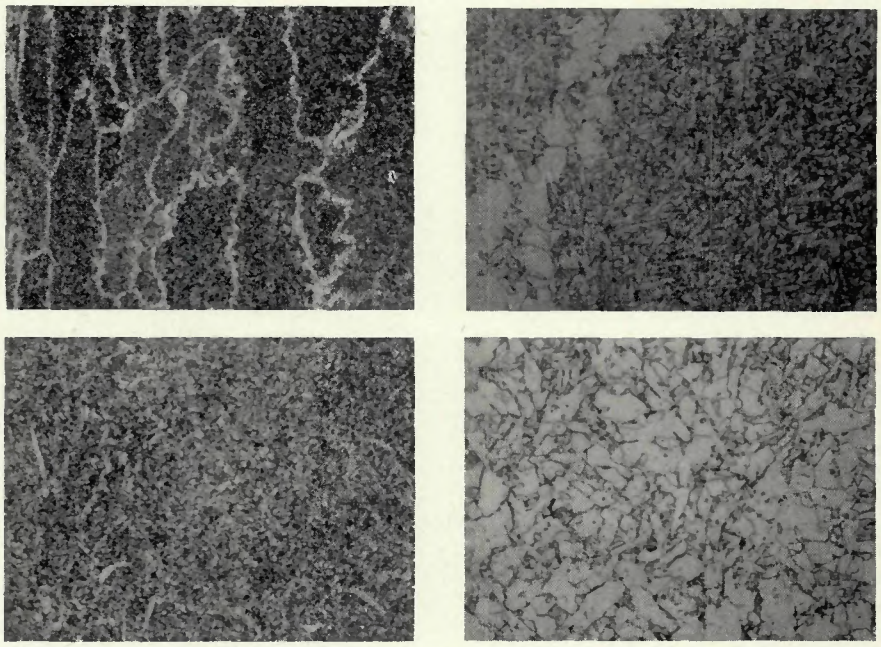

Fig. 5—Alpha-ferrite weld metal microstructures. A (top left)—S-1 in air, X100; B (top right)—S-1 in air, X800; C (bottom left)— SA-1 in air, X100; D (bottom right)—SA-1 in air, X800. A and B are typical also of S-1 in argon, S-2 in air or argon, and ST-1 in air; C and D are also typical of SA-2 in air. Etchant: 2% nital. (reduced 44% on reproduction)

measures matrix titanium concentrations only. Figure 4 illustrates that there are a great many titanium-bearing particles in the weld metals killed with titanium, while there are comparatively few aluminum-bearing particles in welds killed with aluminum. Manganese and silicon-bearing particles are at least as infrequent as aluminum-bearing particles.

Weld Metal Structure

The weld metals exhibit four different microstructures, each characterized by a predominant feature. Considering first the experimental electrodes, the seven welds containing the least amount of killing agents in solid solution (S-1 and S-2 in air and argon and SA-1, SA-2, and ST-1 in air) are characterized by very fine ferrite. Somewhat coarser ferrite (except in the two aluminum containing welds) also outlines what appears to have been prior austenite and/or delta-ferrite grain boundaries—Fig. 5.

Increasing amounts of killing agents in solid solution suppress the austenite to ferrite transformation, so that the seven welds containing higher amounts of killing agents (SA-1 and SA-2 in argon, ST-1 in argon + 7% oxygen, and ST-2 and SAT-3 in air and in argon + 7% oxygen) exhibit bainitic structures. Within this group, there appears to be very little variation in bainite coarseness as the amount of killing agents increase—Fig. 6.

Still further increases in the amounts of killing agents in solid solution suppress the delta-ferrite-to-austenite transformation so that the original large delta-ferrite grains which form upon solidification are retained down to room temperature (welds SAT-1 and SAT-2 in air and in argon + 7% oxygen)—Fig. 7. A similiarity in size and geometry of the grain boundaries of this coarse structure with the outlines in the fine ferrite structure (Fig. 5A) can be noted.

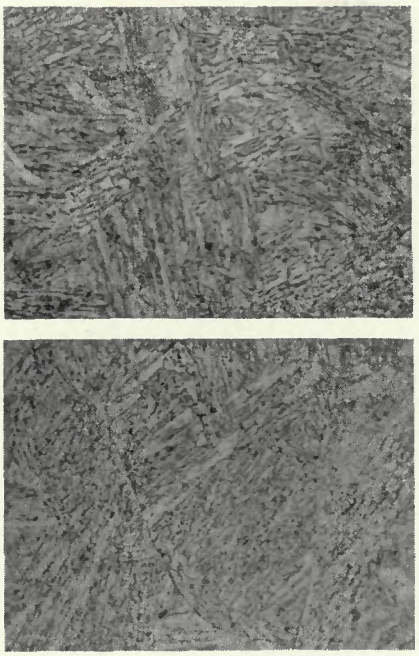

Fig. 6—The range of bainite weld metal microstructure: A (top)—SA-1 in argon; B (bottom)—SAT-3 in argon plus 7% oxygen. These microstructures represent the extremes in bainite coarseness or fineness observed in the test welds. SA-2 in argon, ST-1 in argon plus 7% oxygen, ST-2 in air or argon plus 7% oxygen, and SAT-3 in air are similar to these. Etchant: 2% nital. X800 (reduced 44% on reproduction)

The delta-ferrite grain boundaries of weld SAT-1 in air are almost completely surrounded by bainite. Table 6 indicates that this deposit contains the least amount of killing agents of the four delta-ferrite deposits. Since the killing agents are all ferrite-stabilizers, it is apparent that the three completely delta-ferrite deposits contain enough killing agents to avoid austenite formation entirely. But the deposit of SAT-1 in air is low enough in killing agents to allow a small amount of austenite to form at the delta-ferrite grain boundaries. This then transforms to bainite upon further cooling.

The weld metal deposits from the commercial wire contained a mixed structure of medium-sized ferrite alternated with regions of very fine ferrite-carbide aggregates (possibly bainite)—Fig. 8. Apparently, the mixed microstructure occurs because the weld metal is of such composition that a large part of the metal transforms from delta-ferrite to austenite, and back to ferrite + carbide during cooling. The remaining portion of the metal remained ferrite from solidification to room temperature and therefore became coarser. This hypothesis is supported by an electron probe scan for aluminum (a ferrite stabilizer) and manganese (an austenite stabilizer)—Fig. 9. The unrefined regions are relatively higher in aluminum and lower in manganese than the refined regions.

Mechanical Properties

The hardness, tensile test, and half-thickness Charpy vee notch results of the weld metals are summarized in Table 7. With the experimental electrodes, there is a considerable increase in hardness and tensile strength when the structure changes from fine ferrite to bainite. This is followed by a very marked decrease in hardness and tensile strength as enough killing agent is added to prevent austenite and subsequently austenite decomposition products from forming. The hardness and tensile strength of the commercial electrode deposits are similar to the experimental wire deposits exhibiting fine ferrite.

The Charpy V-notch curves vary considerably with microstructure and composition. Figure 10 illustrates compositional effects when the structure is always fine ferrite. Beginning with the weld metal containing the least amount of killing agent (S-1), there is an increase in transition temperature and a decrease in shelf energy (ductile fracture energy) as aluminum and silicon are added. However, with very small titanium additions

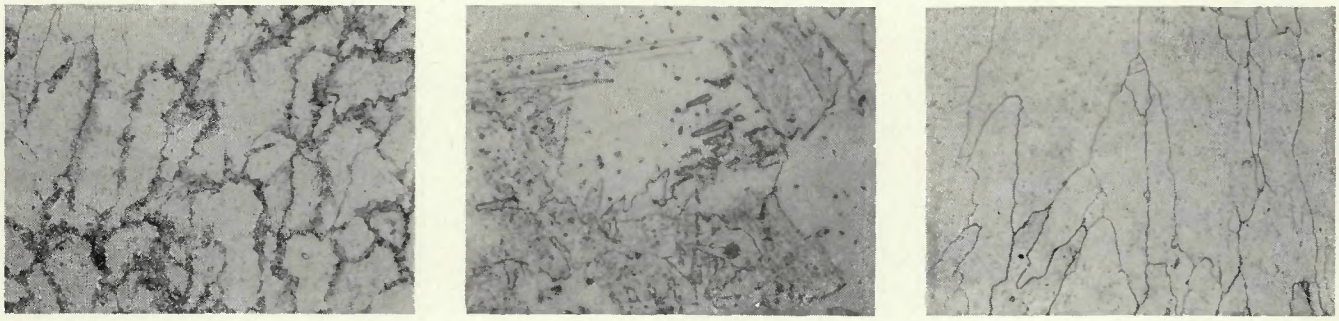

Fig. 7—Delta-ferrite weld metal microstructures: A (left)—SAT-1 in air, X100; B (center)—SAT-1 in air, X800; C (right)—SAT-1 in argon plus 7% oxygen, X100. The dark-etching outlines along most of the delta-ferrite grains in A are shown in B to be bainite. Transformation of SAT-1 in air to austenite appears to have begun at delta-ferrite grain boundaries, then halted by further cooling, causing bainite to form there. C is also typical of SAT-2 in air or in argon plus 7% oxygen. Etchant: 2% nital. (reduced 43% on reproduction)

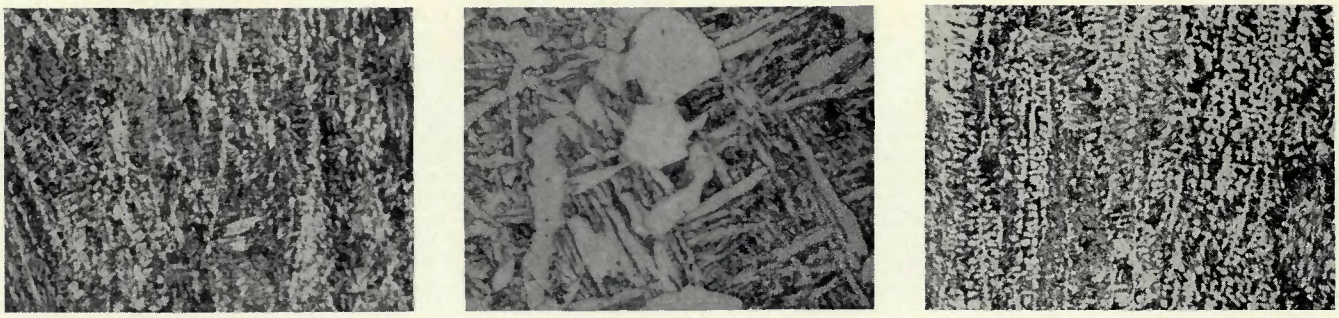

Fig. 8—The mixed microstructure of the commercial electrode deposits: A (left)—welded in air, X100; B (center)—welded in air, X800; C (right)—welded in argon, X100. More of the light-etching constituent (delta-ferrite) is present in the argon-shielded deposit because more aluminum (a ferrite stabilizer) was retained. Etchant: 2% nital. (reduced 43% on reproduction)

(0.03% in solid solution in ST-1) there is a decrease in transition temperature and an increase in shelf energy. The increase in shelf energy apparently results from the more complete deoxidization and denitriding when titanium is present and from the removal of some carbon from solid solution to form titanium carbide.

Figure 11 illustrates the effect of microstructure on the Charpy V-notch curves. Although the amount of killing agents in solid solution increases only slightly (for deposits made from wires SA-1 and ST-1) when switching from air to a shielding gas, it is enough to cause the bainite reaction, and a concomitant large increase in transition temperature.

Figure 12 illustrates the effect of welding in air vs. welding in a nitrogen-free atmosphere for similar microstucture and composition. There appears to be a more detrimental effect (increased transition temperature) in the fine ferrite structure than in the others, but there are also compositional variations present which must be separated and evaluated so that the effect of nitrogen in the arc environment can be evaluated.

Process Considerations

Considering the usability of self-shielded flux-cored electrodes in air, it should be noted that the experimental electrode killed only with silicon are extremely sensitive to voltage. If the open circuit voltage were reduced by 1 v from that listed in Table 5, stubbing of the electrode occurred. On the other hand, if the open circuit voltage were increased by 1 v, macro-porosity appeared. The experimental electrodes with aluminum and/or titanium additions are not so sensitive to voltage, and the commercial electrode is very insensitive to voltage.

Regression Analysis of Results

Regression analysis is a statistical technique which can be used to fit a model to experimental data in such a way as to minimize the lack of fit of the data to a model of a particular form.[14] It has been applied to quantitatively separate the effects of alloy additions and grain size on Charpy V-notch behavior in steels[15] and steel weld metal.[10]

The usual form for such a model would be: Transition temperature (°F) $= A + B_1$ (% Mn) $+ B_2$ (% Si) $+ B_3$ (% Al) $+ B_4$ (% Ti) $+ C$ (grain diameter)$^{-1/2}$. This type of model assumes that the effects on transition temperature of the various alloying elements and of grain size are independent of one another.

For the present study, this form of the model will be modified somewhat. Comparison of Figs. 5–8 reveals that, in these weld metals, a grain size definition capable of describing all four structure types would be rather nebulous. However, it was observed that there is not much difference in microstructure within any of the four major groups. So it was decided to use a model which allows the leading parameter A to take four different values—one for each microstructure type, thereby eliminating the need for a grain diameter term. In effect, grain size is included in the parameter A. This modification requires the assumption that the effects of the various alloying elements are the same for each microstructure type. In the three microstructures which are primarily ferritic, this assumption is similar to that for the more usual form of the model. However, including the bainitic type microstructure makes the assumption more restrictive. An additional term is also included to allow for the effect of air (nitrogen) in the arc environment on transition temperature. Again the assumption is made that the effect is the same from one structure to the next.

Because manganese was not sysmatically varied in the experimental design, the data is ill-suited to estimating the effect of manganese. As a result, it was decided to use the effect of manganese given by Ohwa[10] for steel weld metal deposited by the shielded metal-arc process. His value for this effect on transition temperature is −54° F per weight per cent

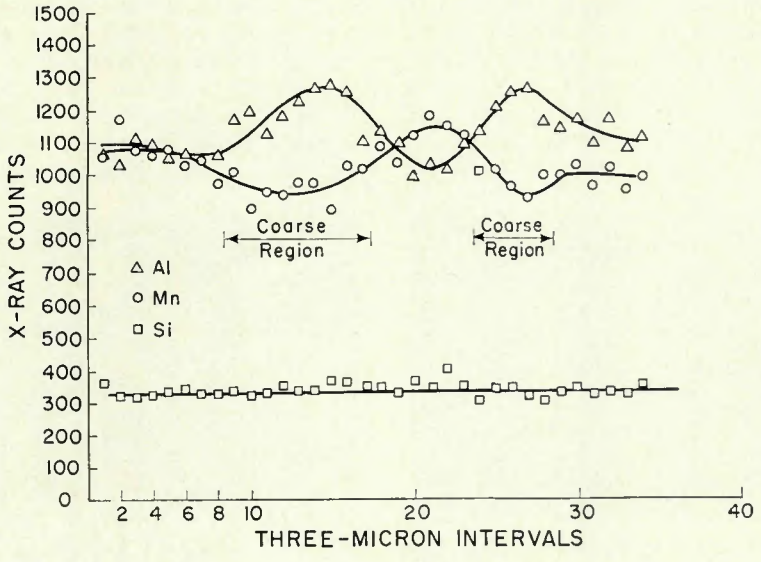

Fig. 9—Electron probe counts at three-micron intervals across the microstructure of the commercial electrode deposited in air. The periodic variations in aluminum and manganese counts correspond to changes in structure. Electron probe operating conditions: 25 kv, 0.03 micro-amp

Table 7—Mechanical Properties of the Deposits

Electrode	Arc environment	Hardness Macro R_B	Hardness Micro DPH	Yield strength (.2% offset), psi	Ultimate tensile strength, psi	Elongation, %	Charpy V-notch shelf energy, ft-lb	Charpy V-notch transition temperatures, °F Mid	15 ft-lb	10 ft-lb
S-1	Argon	92.7	209.2	47.2;[b]	58.8;[b]	18.5;[b]	38	−88	−101	−123
	Air	96.7	260.4	58.1;[a] 59.0[a]	65.9; 69.0	17.3; 14.2	38	−30	−53	−80
S-2	Argon	98.6	237.6	60.5; [b]	76.7; [b]	16.3; [b]	36	−16	−34	−64
	Air	96.9	274.4	57.8; 53.6	76.5; 72.0	13.7; 15.8	32	60	46	6
SA-1	Argon	105.4	321.3	82.8; 82.6	103.7; 99.2	12.6; 10.5	35	86	57	12
	Air	94.7	243.6	68.7; 46.5	76.2; 70.2	14.8; 19.8	26	−8	−2	−50
SA-2	Argon	104.8	311.8	85.4; 79.0	102.4; 100.5	8.9; 11.6	24	202	230	160
	Air	96.8	242.8	56.2; 53.5	79.6; 81.4	16.2; 17.8	28	28	28	−34
ST-1	Argon+7% O_2	101.4	288.3	77.3; 83.3	91.0; 87.5	11.5; 10.0	42	132	120	110
	Air	96.6	252.7	60.1; 55.5[a]	72.5; 67.9	15.1; 14.7	42	−36	−71	−100
ST-2	Argon+7% O_2	103.9	314.4	85.8; [b]	101.5; [b]	10.7; [b]	40	172	144	109
	Air	103.1	310.1	75.8; 63.7	90.6; 76.8	10.7; 11.0	36	164	150	128
SAT-1	Argon+7% O_2	79.4	201.9	20.0; [b]	32.4; [b]	19.9; [b]	50	224	174	146
	Air	85.9	169.5	31.4; [b]	45.3; [b]	13.9; [b]	46	343	277	222
SAT-2	Argon+7% O_2	86.5	205.1	28.7; 25.9	41.8; 40.8	16.2; 19.3	40	286	252	228
	Air	85.3	199.2	25.7; 24.9	40.2; 37.9	18.9; 16.8	50	294	229	196
SAT-3	Argon+7% O_2	104.8	298.7	86.0; 103.3	106.0; 108.5	10.3; 8.2	32	187	175	124
	Air	102.5	278.1	72.5; 76.2	88.2; 92.0	10.7; 12.6	33	155	139	116
Commercial	Argon	96.5	245.6[d] 285.7	51.9; [b]	82.0; [b]	19.1[c]; [b]	40	142	113	82
	Air	94.8	252.3[d] 288.7	43.4; 43.8	64.2; 63.3	23.3[c]; 20.5[c]	36	142	128	108

[a] Specimen exhibited upper and lower yield points. Data presented is lower yield point.
[b] Specimen contained an obvious defect and therefore was not tested.
[c] Shorter gage length—3/4 in. vs. greater than 0.9 in.
[d] Dual microstructure. Smaller number on delta-ferrite.

manganese. The form of the model to be fit then is:

$$\text{Transition temperature (°F)} = A - 54(\%\ \text{Mn}) + B_2(\%\ \text{Si}) + B_3(\%\ \text{Al}) + B_4(\%\ \text{Ti}) + D\ (\text{if used in air})$$

Three different ways of measuring transition temperature were considered:

1. The temperature at which the Charpy V-notch energy curve passes though the average energy of the transition range, i.e., the midpoint energy between fully brittle and fully ductile fracture energies.

2. The temperature at which the Charpy V-notch energy curve passes through 15 ft-lb.

3. The temperature at which the Charpy V-notch energy curve passes through 10 ft-lb.

These transition temperatures for each weld metal have been tabulated in Table 7.

During the course of developing and fitting this model, it was observed that the transition behavior of one weld (SAT-1 in air) seemed markedly out of order compared to the other three welds of the delta-ferrite structure group, and as a result was distorting the model. Examination of its properties listed in Table 7 and comparison of these properties with the other delta-ferrite weld metals demonstrates this. These observations plus the structural differences noted in this weld compared to the other delta-ferrite weld metals (Fig. 7) resulted in the decision to omit the data from the final fit of the model.

The chemical composition data used in obtaining the models were initially taken from the electron probe data, since solid solution effects were being sought. The parameters obtained by regression analysis with the aid of a digital computer are presented in Table 8. This was then compared with the parameter estimates obtained from the bulk analysis data, which are presented in Table 9.

There is a good deal of consistency between the parameter estimates obtained from electron probe solid solution measurements and those from the

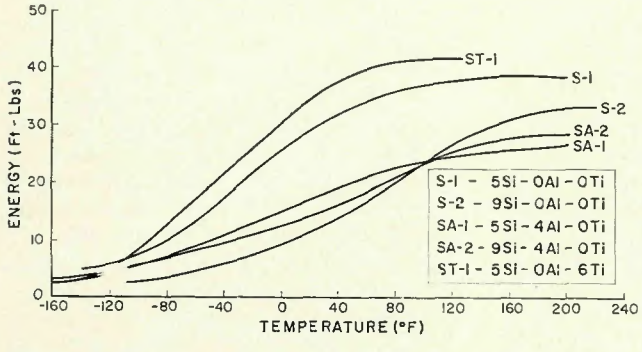

Fig. 10—Charpy V-notch energy as a function of temperature for test welds made in air, all having the alpha-ferrite microstructure

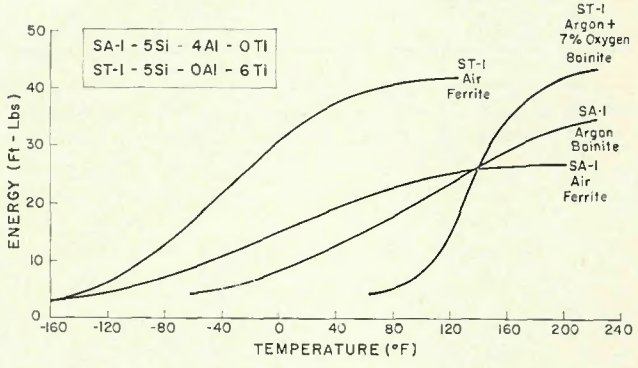

Fig. 11—Charpy V-notch energy as a function of temperature for electrodes SA-1 and ST-1 showing the effect of changes in microstructure. The retention of more killing agent when the electrodes were used in a nitrogen-free arc environment caused the microstructure to change from the alpha-ferrite that was obtained in air to bainite

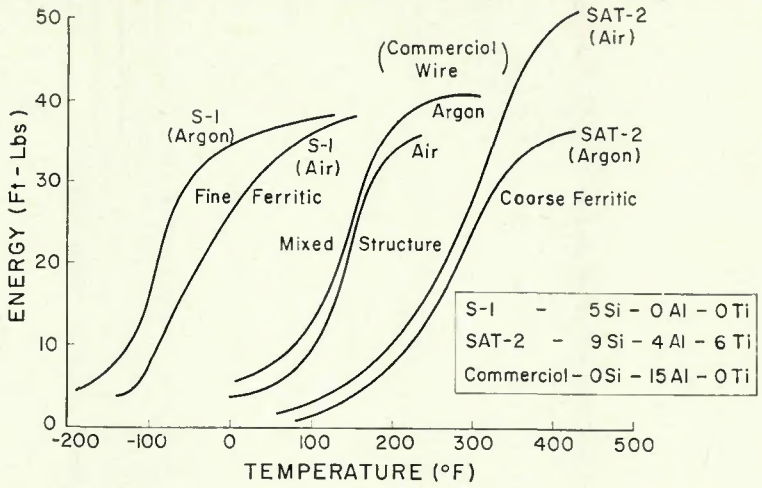

Fig. 12—Charpy V-notch energy as a function of temperature for electrodes S-1, ST-2, and the commercial electrode, showing the effect of air, when the resulting microstructure in air is the same as the microstructure obtained in a nitrogen-free arc environment

bulk analyses. The most notable exception is in the estimates of the titanium effect, because as mentioned previously titanium-bearing particles as well as titanium dissolved in the matrix is considered when bulk analyses are made.

There appears to be little preference from a statistical point of view for one set of parameter estimates over another. The standard deviation shows little change, the range being from 28 to 38° F. The authors feel a preference for the midpoint method of measuring transition temperature because a specific energy level like 15 ft-lb may be closer to a fully brittle fracture in one weld compared to another depending on the relative levels of ductile fracture energy. The authors also feel a preference for the probe method of measuring chemical composition because it allows a direct measurement of the degree of solid solution effects of a given element independent from particle analysis.

Summarizing then, the authors preferred form of the model is:

Midpoint transition temperature
(°F) = A − 54 (% Mn)
+ 98.9 (% Si) + 36.5 (% Al)
+ 155 (% Ti) + 24 (if used in air).

The parameter A depends upon microstructure. For fine grained ferrite the value A is −37.9° F. For the other structures observed in this study, A takes on values of about 100° F or more.

Table 8—Parameter Estimates Obtained by Regression Analysis of Electron Probe Solid Solution Data, Assuming Constant Effect of Manganese of −54° F/% Mn

Transition measured by:	Midpoint	15 ft-lb	10 ft-lb	Standard deviation of estimate, ESD's
A (alpha-ferrite), °F	−37.9	−67.3	−79.1	0.954
A (bainite). °F	101.5	63.2	63.7	1.31
A (delta-ferrite), °F	124.0	19.9	57.0	2.95
A (mixed structure), °F	97.7	21.6	88.4	2.23
B_2, °F/%Si	98.9	111.9	92.5	0.835
B_3, °F/%Al	36.5	65.9	16.4	1.135
B_4, °F/%Ti	155.0	185.1	178.0	3.95
D, °F when air is present	24.0	22.4	23.1	0.515
Estimated standard deviation (ESD), °F	28.0	37.2	32.7	

Table 9—Parameter Estimates Obtained by Regression Analysis of Bulk Analysis Data, Assuming Constant Effect of Manganese of −54° F/% Mn

Transition Measured by:	Midpoint	15 ft-lb	10 ft-lb	Standard deviation of estimate, ESD's
A (alpha-ferrite), °F	−36.2	−63.8	−79.4	0.973
A (bainite), °F	109.9	85.7	72.3	1.261
A (delta-ferrite), °F	164.2	122.9	115.6	3.255
A (mixed structure), °F	132.3	93.6	133.2	2.22
B_2, °F/% Si	104.0	120.5	101.8	0.838
B_3, °F/% Al	21.4	30.1	−4.1	1.272
B_4, °F/% Ti	57.7	6.7	48.5	3.54
D, °F when air is present	17.5	15.8	13.9	0.529
Estimated standard deviation (ESD), °F	31.7	35.8	32.1	

Conclusion

Several useful conclusions can be drawn from the previously postulated model despite its limitations in accuracy. First, it is essential that killing agent additions to the electrode core be kept low so that the amount of killing agents entering solid solution will be small enough to permit formation of fine-grained ferrite. The "penalty" for obtaining any of the other structures found in this study can be increases in transition temperature greater than 100° F.

The experimental results (Table 8) indicate that, of the killing agents studied, silicon has the least ability to promote the bainite reaction, and titanium the greatest. This is consistent with the effects of silicon, aluminum, and titanium on their binary phase diagrams with iron—that is, 2.15% silicon prevents austenite formation in iron-silicon alloys, 1.2% aluminum prevents austenite formation in iron-aluminum alloys and only 0.75% titanium prevents austenite formation in iron-titanium alloys.[16] The actual silicon, aluminum, or titanium tolerance of the weld metal depends on other factors such as manganese and carbon content (since these elements also increase the tendency to form bainite) and on interpass temperature (since this affects the cooling rate).

For a given structure, aluminum exerts the least detrimental effect on transition temperature, and titanium the most. The numerical values for the silicon effect in the models (86 to 120° F/% Si) is more consistent with the reported effect of Rinebolt and Harris[9] (125° F/% Si) for wrought material than with that of Ohwa[10] (14° F/% Si) for weld metal. Beneficial, rather than detrimental effects of aluminum and titanium on transition temperature have been reported by these same researchers, but the levels

considered were much lower and, in addition, no attempts were made to distinguish between the amounts of these elements in solid solution or in particles.

Another factor to consider in the selection of killing agents is their effect on ductile fracture energy. In this study, deposits killed with aluminum and silicon possessed the lowest shelf energy. The highest ductile fracture energies were obtained with titanium additions.

In comparison to the two-fold effect of killing agents (increasing transition temperature for a given structure and promoting formation of brittle structures), the effect of air in the arc environment seems small—on the order of a 25° F increase in transition temperature. However, this effect may be greater in the tougher fine-grained ferrite structure.

The only two electrodes exhibiting the fine-grained ferrite structure in both air and argon were S-1 and S-2. Their midpoint transition temperatures increased by 58 and 76° F respectively when welded in air vs. argon. If the effect is really this large for the fine-grained ferrite structure and very small for the brittle structures, it would be masked by the assumption that it is the same for all structures. Further study of electrodes forming only fine-grained ferrite seems warranted from a design point of view for this reason and because this was the toughest structure obtained.

The Toughness Study—Part II

In the second part of this study, an attempt will be made to determine quantitatively the ability of the three killing agents, namely silicon, aluminum and titanium, to prevent formation of the tough fine-grained ferrite structure.

A study of Charph V-notch fracture surfaces will be made by electron fractography to relate fracture characteristics with microstructure and inclusions. The particles present on the fracture surface will be identified by electron probe analysis.

Acknowledgments

The authors are particularly indebted to Dr. D. C. Smith and his associates of the P & H Welding Products Unit, first of Harnischfeger Corporation and now of Chemetron Corporation, who counseled the authors concerning electrode flux chemistry, fabricated the experimental electrodes used in this study, and performed bulk chemical analysis on the weld deposits.

The authors are also grateful to Mr. E. D. Glover of the Geology Department of the University of Wisconsin for his counsel during electron probe analysis and to the United States Steel Corporation which provided the vacuum melted steel base metal used in this study.

The graduate student author was supported in part during the time of this study by an NDEA Title IV fellowship and by scholarships from the Milwaukee Section of the American Welding Society.

References

1. Smith, D. C., "Development, Properties and Usability of Low-Hydrogen Electrodes." WELDING JOURNAL, 38 (9), Research Suppl, 37-s to 392-s (1959).
2. MacShane, G. H., and Reid, H. F., "Tubular Electrodes—Firm Round and Fully-Packed," *Ibid.*, 45 (2), 116 to 122 (1966).
3. Wilson, R. A., "Vapor-Shielded Arc Welding at 200 IPM," *Ibid.*, 40 (1), 13 to 17 (1961).
4. Landis, G. G., and Patton, D. M., "Method and Means of Bare Electrode Welding," U. S. Pat. 2,909,778, 10-20-59, The Lincoln Electric Co.
5. Smith, D. C., and Johannes, K. P., "Development of a Notch-Tough Self-Shielded Flux-Cored Electrode," WELDING JOURNAL, 47 (3), 207 to 214 (1968).
6. Chin, L. L-J., "A Model for Toughness Studies of Welds," *Ibid.*, 48 (7), Research Suppl., 290-s to 294-s (1969).
7. Wheatly, J. M., and Baker, R. G., "Mechanical Properties of a Mild Steel Weld Metal Deposited by the Metal Arc Process," *British Welding Journal*, June 1962, pp. 378-387.
8. Crussard, C., Borione, R., Plateau, J., Morrillon, Y., and Maratray, F., "A Study of Impact Tests and the Mechanism of Brittle Fracture," Journal of the Iron and Steel Institute, V.182 (June 1956), pp. 146-177.
9. Rineholt, J. A., and Harris, W. J., Jr., "Effects of Alloying Elements on Notch Toughness of Pearlitic Steels," *Trans. ASM*, V.43 (1951), pp. 1175-1214.
10. Ohwa, T., "Statistical Investigation on the Effect of Alloying Elements for the Notch-Toughness of Weld Metals," Document 11-221-62, Commission II of the International Institute of Welding (1962).
11. Philibert, J., *3rd International Symposium on X-Ray Optics and X-Ray Microanalysis*, Stanford, New York: Academic Press, 1962, p. 379.
12. Reed, S. J. B., "Characteristic Fluorescence Corrections in Electron-Probe Microanalysis," *British Journal of Applied Physics*, V.16 (1965), pp. 913-926.
13. Thomas, P. M., "A Method of Correcting for Atomic Number Effects in Probe Microanalysis," *Atomic Energy Research Establishment Report No. 4593.*
14. *The Design and Analysis of Industrial Experiments*, O. L. Davies, Oliver and Boyd, London, 1963, pp. 566-578.
15. Pickering, F. B., and Gladman, T., "Metallurgical Developments in Carbon Steels," British Iron and Steel Research Association Report 81 (1963), p. 9.
16. Hansen, M., *Constitution of Binary Alloys*, McGraw-Hill, New York, 1958, pp. 91, 713, 725.

WRC Bulletin No. 148 Feb. 1970

"Interaction Curves for Sections Under Combined Biaxial Bending and Axial Force"

By S. Santathadaporn and W. F. Chen

In this study, carried out at Lehigh University, limit analysis was applied to obtain interaction equations for rectangular and wide-flange sections under combined biaxial bending and axial force. Some of the results are presented in terms of interaction curves and comparisons are made for various weights and sizes of commonly used wide-flange sections.

The theory applied in this project should be considered as a first step in extending planer structural analysis and design to a more realistic space from analysis and design.

The price of Bulletin 148 is $1.00 per copy. Orders should be sent to the Welding Research Council, 345 East 47th St., New York, N. Y. 10017.